Anisotropy in particle orientation controls water diffusion in clay materials

Eric Ferrage, Fabien Hubert, Thomas Dabat, Ali Asaad, Baptiste Dazas, Brian Grégoire, Sébastien Savoye, Emmanuel Tertre

Anisotropy in particle orientation controls water diffusion in clay materials

Eric Ferrage[a]*, Fabien Hubert[a], Thomas Dabat[a], Ali Asaad[a], Baptiste Dazas[a], Brian Grégoire[a], Sébastien Savoye[b], Emmanuel Tertre[a]

[a] *IC2MP, Equipe HydrASA, UMR 7285 CNRS/Université de Poitiers, 86073 Poitiers, France,*

[b] *Université Paris-Saclay, CEA, DRMP-Service de Physico-Chimie, 91191 Gif-sur Yvette, France*

*Correspondence e-mail: eric.ferrage@univ-poitiers.fr

Abstract

Clay minerals are used in a wide number of natural or artificial materials for municipal or nuclear waste management in which water diffusion is the principal transfer process. However, a quantitative assessment of the impact of the preferred orientation of lamellar clay particles on water diffusion is still lacking. Using 3D Brownian dynamics simulation on representative virtual clay porous media, a systematic study of water diffusion for single-porosity (illite or kaolinite) and dual-porosity (vermiculite) systems was conducted. The simulated water diffusion coefficients were validated through comparison with experiments and were used to build an Archie model including the degree of anisotropy in particle orientation. The results showed that water diffusion can be predicted based on a correct description of the solid phase organization and that clay particle orientation, such as interparticle porosity, is a primary parameter governing water mobility. Moreover, the anisotropy of water diffusion can be linked to the degree of particle preferred orientation, irrespective of the porosity value. The modified version of the Archie model for water diffusion in clay systems proposed here has many potential applications where decoupling of porosity and preferred orientation is needed, including better prediction of water transfers or improved designs of clay liners with sustainable use of natural mineral resources.

Keywords: clay minerals; water diffusion; porous media, Brownian dynamics; Archie model

Highlights

- 56 virtual porous media differing in porosity or particle orientation are generated
- Brownian dynamics water diffusion simulations are validated against experiments
- Anisotropy in water diffusion is directly correlated to particle orientation
- A predictive Archie model, including porosity and particle orientation, is proposed

1. Introduction

Clays are naturally occurring lamellar minerals commonly found in most natural systems, such as soils, sediments, or rocks. Their high adsorption properties make them responsible for the fate of a wide range of inorganic or organic pollutants in natural media, including emerging micropollutants (Yan et al., 2021; Yang et al., 2022; Ye et al., 2022). The surface properties of clays are also at the origin of the use of clay minerals for water treatment as well as for municipal or nuclear waste repositories (Charlet et al., 2017; Czurda, 2006; Das and Bharat, 2021; Mazurek et al., 2008; Nakazawa et al., 2021; Wang et al., 2021). In these latter repositories applications, the migration of polluted water is expected to be reduced due to interaction with clay surfaces. Furthermore, owing to their small particle size, clay-rich materials display low permeability values. The transfer of polluted water is thus further limited but remains possible solely through diffusion processes.

Understanding the water diffusion process in clay materials is of prime importance for the prediction of water quality and for risk assessment in the case of hazardous waste management. Water is the principal vector of migration of aqueous pollutants and in the case of nuclear waste management, understanding and predicting water mobility is a key and reference parameter in environmental migration models. Other solutes (i.e., anions and cations) are in addition influenced by electrostatic interaction occurring in the diffuse double layer located at the vicinity of the clay surfaces (Bourg and Tournassat, 2015; and literature therein).

The effective diffusion coefficient D_e is commonly used for characterizing the diffusing properties of species in porous media (Charlet et al., 2017; Glaus et al., 2010; Kim and Chen, 2006; Van Loon et al., 2005, 2005; Wu et al., 2018, 2014, 2012). This key parameter is most often derived from macroscopic diffusion experiments, such as through-diffusion experiments, and depends on the average bulk properties of the material, such as the porosity ε and tortuosity τ. The porosity ε accounts for the accessible relative volume for diffusion of water molecules. The tortuosity parameter τ represents the pathway ratio between the shortest linear distance between the original and final migration points compared to that used by the molecules through the pore network. All these entities are connected through the following equations:

$$D_e = \varepsilon.\tau.D_0 = \varepsilon.D_p \quad , \quad (1)$$

where D_0 is the self-diffusion coefficient of water in bulk water and D_p is the pore self-diffusion coefficient of water in the investigated material. For macroscopic operational description and prediction of water (and other species) diffusion in clay systems, the dependence of the D_e parameter on ε is commonly quantified through an empirical relationship named Archie's law. This power law is derived from the relation originally proposed (Archie, 1942) for the porosity dependence of electrical conductivity and takes the form:

$$D_e/D_0 = \varepsilon^m \quad , \quad (2)$$

where m is referred to as the cementation factor (Charlet et al., 2017; Descostes et al., 2008; Glaus et al., 2010; Van Loon et al., 2005, 2005; Wu et al., 2018, 2014, 2012). In Eq. (2), the m parameter ranges between 2 and 6 (Charlet et al., 2017; Mazurek et al., 2008; Van Loon and Mibus, 2015), as determined from a large body of experiments on reference clays and clay-rich media. Several alternative empirical expressions of the Archie relation for diffusion in clay porous media were also proposed based on both experimental and numerical studies, such as:

$$D_e/D_0 = A.\varepsilon^m \quad (3)$$

with A an additional empirical factor (Rosanne et al., 2003; Tyagi et al., 2013). According to the Archie empirical description, ε is the primary parameter governing the diffusion of water, whereas m and/or A parameters includes a large number or geometric and geochemical effects.

As far as water diffusion is concerned, geometric effects and associated tortuosity of the pore network represents a first-order parameter controlling the mobility of water tracers. Firstly, clay-rich systems, such as clayrock most often show contrasting diffusion properties between the normal and in-plane directions of compaction (Gimmi et al., 2014; Robinet et al., 2012; Van Loon et al., 2004; Van Loon and Soler, 2004). Part of this diffusion anisotropy is related to the presence of elongated non-clay particles (Robinet et al., 2012), whereas preferential orientation of clay particles is commonly suspected to also enhance this effect (Gimmi et al., 2014; Robinet et al., 2012; Tyagi et al., 2013; Van Loon et al., 2004; Wenk et al., 2008). Indeed, due to their lamellar shape, preferential orientation of clay particles most often induces anisotropy in the diffusional pathway for water and solutes, with a reduction in diffusion in the direction perpendicular to the main orientation of particles. In this context, recent experimental results showed that varying the anisotropy of preferred clay particle orientation in pure clay systems (kaolinite or vermiculite) with constant porosity can significantly affect the diffusion coefficients of water (Asaad, 2021; Dabat et al., 2020). Secondly, clay minerals are known to exhibit different surface charges and different classes of porosities, which in turn govern the swelling nature of the mineral and the number of nearby neutralizing cations whose hydration provokes a decrease in water mobility. For instance, kaolinite clay mineral is a non-swelling and non-charged clay mineral (Fig. 1a). For this mineral, water mobility is thus almost solely governed by diffusion in the interparticle porosity $\varepsilon_{interp.} = \varepsilon$ (Fig. 1b). In contrast, illite is a non-swelling clay mineral with a charged surface (Fig. 1a), and for such a single-porosity medium, water mobility can be slightly reduced close to the surface due to water dipole interaction (Figs. 1b-c; Bourg and Sposito, 2011; Bourg and Tournassat, 2015; Holmboe and Bourg, 2014; Tinnacher et al., 2016). This mobility reduction can be enhanced for low porosity conditions, as surfaces are closely packed and can lead to the presence of nanopores. An extreme case concerning the presence of nanopores is represented by vermiculite clay minerals (Fig. 1a). Like smectite, vermiculite is a swelling and charged clay mineral that exhibits a

defined interlayer nanoconfinement of water with strongly reduced mobility (Michot et al., 2012; Tertre et al., 2021). Clay-rich media containing swelling clays is commonly referred to as a dual-porosity medium with a diffusivity connection between interparticle $\varepsilon_{interp.}$ and interlayer $\varepsilon_{interl.}$ porosities (with $\varepsilon = \varepsilon_{interp.} + \varepsilon_{interl.}$; Figs. 1b-c). Kaolinite, illite, and vermiculite thus well illustrate that porosity can be of different natures in clays, whose effect on the overall tortuosity and water mobility reduction can be enhanced when decreasing porosity to very low values.

The present study aims at exploring the combined influence of porosity and anisotropy in particle orientation on the diffusion of water in both single- and dual-porosity clay media, in an effort to quantitatively decouple respective roles of these parameters on the overall mobility of water tracers. In that perspective, this work benefits from recent diffusion experiments of water tracers on pure kaolinite, illite, and vermiculite samples over a wide range of porosities and degrees in the preferred orientation of particles (Asaad, 2021; Asaad et al., 2021; Dabat, 2019; Dabat et al., 2020, 2019; Tertre et al., 2018). This large set of experimental data is used here as a first objective to experimentally validate water diffusivity derived from three-dimensional Brownian Dynamics (BD) simulations in virtual porous media mimicking the size, shape, and organization of these clay particles in the samples (Asaad et al., 2021; Dabat et al., 2020, 2018; Ferrage et al., 2018, 2015). The second objective of this study is to benefit from the large set of numerical data over a wide range of porosities and degrees in the preferred orientation of particles to better quantitatively assess and generalize the respective role of porosity and preferred orientation of clay particle on water mobility using a modified version of Archie relation.

2. Materials and methods

2.1. Clay samples, preferred orientation measurements and water diffusion experiments

The set of experimental data used in this study is derived from recent measurements of porosity, water diffusion coefficient, and degree of preferred orientation of particles on different pure clay minerals. The clay minerals selected for analysis include kaolinite, illite, and vermiculite, which have distinct surface properties and nano-confinement characteristics (Table 1; Fig. 1a). The kaolinite sample was KGa-2 from the Source Clay Repository of the Clay Mineral Society (Dabat et al., 2020), whereas the illite and vermiculite samples correspond to the 0.1-0.2 µm size fractions of illite du Puy (Asaad et al., 2022) and vermiculite Santa Olalla (Reinholdt et al., 2013), respectively. All samples were Na-saturated (Reinholdt et al., 2013). Note that previous studies have shown a similar aspect ratio (i.e., ratio between mean height and diameter of particles) of approximately 0.1 for these three types of clay minerals (Asaad et al., 2022; Reinholdt et al., 2013; Sayed Hassan et al., 2006).

Different sample preparations, i.e., compaction of dried powders or centrifugation of clay dispersions, were used to obtain different degrees of preferred orientation in clay particles for a given ε value. Quantification of the preferred orientation of particles was systematically achieved through the $\langle P_2 \rangle$ order parameter by analyzing the intensity distribution on a bidimensional X-ray scattering pattern collected on a slice of indurated samples (Table 1; Asaad, 2021; Asaad et al., 2021; Dabat, 2019; Dabat et al., 2020; Tertre et al., 2018). This $\langle P_2 \rangle$ order parameter can indeed be extracted from the scattered intensities (I) along the 001 Bragg peak of the given clay type as a function of the angle ζ on the 2D detector. For low values of Bragg angles (the case of clay minerals), the $I(\zeta) = I(\theta)$ approximation can be used, where θ is the angle between the normal of the particle and the z-axis of the sample (Fig. 1d; Dabat et al., 2019). The distribution of particle orientation, referred to as the orientation distribution function (ODF), is then directly calculated from the scattered intensity $I(\theta)$ as:

$$f(\theta) = \frac{I(\theta)}{\int_0^{\pi} I(\theta) sin(\theta) d\theta} \quad , \tag{4}$$

and the $\langle P_2 \rangle$ order parameter is calculated as:

$$\langle P_2 \rangle = \int_0^{\pi} P_2(cos\theta).f(\theta) sin(\theta) d\theta \quad , \tag{5}$$

where $P_2(cos\theta)$ is the second-order Legendre polynomial. The $\langle P_2 \rangle$ order parameter is very convenient to quantify the degree of preferred orientation of clay platelets, as it can take a value between 0 for an isotropic particle organization and 1 for perfectly anisotropic organization with all particles having the same orientation.

The experimental water diffusion coefficients for kaolinite, illite, and vermiculite used in this study and reported in Table 1 were obtained using a combination of methods, including through-diffusion (TD) experiments of HDO water tracers and ^{1}H pulse-gradient spin–echo nuclear magnetic resonance (PGSE-NMR) spectroscopy. TD experiments allow determining the effective diffusion coefficient of water traversing a centimetric sample in the direction perpendicular to the sedimentation plane of the particles (i.e., D_{ez}; Figs. 1b-c). In contrast, the analysis of pulsed gradient spin echo attenuation measurements by the PGSE-NMR technique provides information regarding the pore self-diffusion of individual water probes in the scalar direction of the sample (i.e., D_{px}, D_{py}, D_{pz}; Figs. 1b-c;(Dabat et al., 2020; Porion et al., 2018). Pore self-diffusion of water derived from the PGSE-NMR technique can then be compared to the effective diffusion coefficient obtained from TD measurements through the relation given in Eq. (1). Despite the fact that these two independent techniques probe different length and time scales (i.e., several days for TD vs. several milliseconds for PGSE-NMR; Asaad et al., 2021; Glaus et al., 2010; Porion et al., 2021, 2018; Tertre et al., 2018), a recent study by Asaad et al. (2021) showed that experimental water diffusion coefficients were consistent using both methods.

2.2. Brownian dynamics simulations of water diffusion on 3D virtual porous media

The water dynamics were investigated based on Brownian dynamics (BD) simulations in both single-porosity and dual-porosity clay media using original 3D virtual porous media (VPM) using homemade program (Ferrage et al., 2015). The basic description of the methodology used for the generation of these VPM, mimicking the distribution of the shapes and sizes of individual clay particles in the porous medium, has been extensively described elsewhere (Asaad et al., 2021; Dabat et al., 2020, 2018; Ferrage et al., 2018, 2015). Briefly, the particles are allowed to settle in a square simulation box with periodic conditions along the *x*- and *y*-axes (*z*-axis pointing upward; Fig. 1d) according to a steepest descent algorithm to reduce the barycenter altitude. A log normal distribution in the dimensions (i.e., basal surface, particle diameter, ratio between thickness and diameter, and ellipticity degree) of the individual particles was obtained from the work of Ferrage et al. (2015) and based on an experimental morphological study Reinholdt et al. (2013) for the 0.1-0.2 μm size fraction of vermiculite from Santa Olalla, Spain. During the settling process, particles are allowed to slide, swivel or rotate with a random amplitude that ranges from zero to a maximum value. A wide range of degrees of anisotropy in the particle orientation is then obtained by tuning the amplitudes of the movements, leading to a variation in the degrees of freedom in the particle motions (Ferrage et al., 2015). For the experiments, the degree of preferred orientation was then quantified through the $\langle P_2 \rangle$ parameter calculated, as for Eq. (5), as the average of the second-order Legendre polynomial on the angular distribution of the particle orientations:

$$\langle P_2 \rangle = \int_0^{\pi} P_2(cos\theta).\,\mathrm{g}(\theta) d\theta \quad (6)$$

where θ is the angle between the normal unit vector of the particle and the *z*-axis of the simulation box (Fig. 1d), and $\mathrm{g}(\theta)$ the angular distribution function of particles in the VPM (with $\int_0^{\pi} \mathrm{g}(\theta)\, d\theta = 1$). As detailed by Dabat et al. (2020), additional treatments can be applied to allow BD simulations on VPM with a wide range of porosity values. These treatments included cubic periodic conditions in the *x*, *y*, and *z* directions of the simulation box and a process of injection and growth of additional particles. The final VPM was rescaled so that the mean particle size and thus the mean specific surface areas were similar for all VPMs. Compared to previous studies of Dabat et al. (2020) and Asaad et al. (2021), the number of VPM was largely extended in the present work up to 56 VPM with $\langle P_2 \rangle$ and $\varepsilon_{interp.}$ parameter values varied from 0.03 to 0.96 and from 0.20 to 0.60, respectively (Table S1), thus allowing us to investigate the water dynamics as a function of $\langle P_2 \rangle$ for the same ε value (Fig. 1e) or as a function of ε for the same degree of preferred orientation (Fig. 1f). The total number of particles ranges between ~1700 and ~12000, depending on the $\langle P_2 \rangle$ and $\varepsilon_{interp.}$ values (Table S1) for a simulation box with final cubic lengths of ~1 μm.

For all generated VPMs, the BD simulations were performed according to the methodology detailed by Dabat et al. (2020) or Asaad et al. (2021) in the case of water diffusion in single-porosity or dual-porosity media, respectively. Briefly, in the specific case of independent displacements of probes i, with a time step δt much larger than the velocity correlation time γ_i (i.e., $\gamma_i \delta t \gg 1$), the displacement of molecular probes in the framework of the general Langevin equation can be simplified as (van Gunsteren et al., 1981):

$$\vec{x}_i(t + \delta t) = \vec{x}_i(t) + \vec{R}_i \quad , \tag{7}$$

with $\vec{R}_i$ as a random force that satisfies a Gaussian displacement distribution function with zero mean and standard deviation as given by:

$$\langle {R_i}^2 \rangle = 2 D_i \delta t \quad . \tag{8}$$

where D_i is the molecular self-diffusion of probe i. The density of the probability of the displacement distribution law, i.e., the self-diffusion propagator, is then defined as (Asaad et al., 2021; Bacle et al., 2016; Callaghan, 1991; Chandrasekhar, 1943; Dabat et al., 2020):

$$P(\vec{r}, \Delta \mid \vec{r}_0 \ ,0) = \{4\pi D \Delta\}^{-3/2} exp\left[-\frac{(\vec{r}-\vec{r}_0)^2}{4D\Delta}\right] \quad , \tag{9}$$

where Δ is the diffusion time. The 3D self-diffusion propagator that quantifies the mobility along a single $\overrightarrow{e_\alpha}$ director is then defined by:

$$P_\alpha(\overrightarrow{r_\alpha}, \Delta \mid \overrightarrow{r_{\alpha_0}}, 0) = \{4\pi D_\alpha \Delta\}^{-1/2} exp\left[-\frac{\left(\overrightarrow{r_\alpha}-\overrightarrow{r_{\alpha_0}}\right)^2}{4D_\alpha \Delta}\right] \quad , \tag{10}$$

where D_α is the component of the self-diffusion tensor that describes the mobility of the probe along the selected $\overrightarrow{e_\alpha}$ director (Callaghan, 1991).

Based on this fundamental description of the diffusion process, two distinct sets of BD simulations were performed to predict water diffusion properties in single-porosity or dual-porosity media, respectively.

For single-porosity systems (i.e., kaolinite and illite; Fig. 1a), water diffusion occurs only in the interparticle pore space $\varepsilon = \varepsilon_{interp.}$. A number N = 2000 of water probes with molecular self-diffusion $D_{interp.} = D_0$ = 2.3.10^{-9} m^2.s^{-1} were randomly introduced into the interparticle porosity of the VPM. The time step δt was set at 200 ps over a total simulation time of 0.12 ms, as additional tests with smaller values for δt did not show a difference in the simulation results (Asaad et al., 2021). During the simulations, the collision with the surfaces of particles was treated in the framework of Maxwell's A wall (Valleau et al., 1991), according to water probes have an uniform angular probability of rebounding from the surface of particles (Dabat et al., 2020). This mimics the trajectory of a molecule by assuming a residence time at the solid surface that is long enough to thermalize its velocity distribution function before being desorbed and returning to the fluid. The pore water diffusion coefficients Dp_α along a selected $\overrightarrow{e_\alpha}$ director

was finally extracted from the asymptotic slope of the radial mean squared displacement as follows:

$$Dp_\alpha = \lim_{\Delta \to \infty} \frac{\sum_{i=1}^{N} \left(x_{i,\alpha}(0) - x_{i,\alpha}(\Delta) \right)^2}{2N\Delta} \quad , \tag{11}$$

where α refers to the single direction $\overrightarrow{e_\alpha}$ on which the mobility is extracted (other parameters already defined above; uncertainty on the calculated Dp_α values estimated at 15%). Despite the fact that the VPM was designed to mimic vermiculite particles, this type of simulation is also fully representative for illite and kaolinite samples. Particles for these three types of minerals indeed display similar particle aspect ratios (i.e., the ratio between the particle thickness and diameters of ~0.08, ~0.08, and ~0.07 for vermiculite, illite, and kaolinite, respectively (Asaad et al., 2022; Reinholdt et al., 2013; Sayed Hassan et al., 2006). Moreover, the computed water diffusion in single-porosity systems as performed here is independent of the particle size, which is similar for vermiculite and illite (i.e., 0.1-0.2 µm size fraction), whereas kaolinite displays larger particle dimensions. Indeed, according to the BD simulations considered here that do not consider specific interfacial effects on the probe dynamics, the water mobility is independent of the mean particle size, given that the time step δt is correctly chosen in Eq. (8) and that the overall diffusion time Δ is sufficient to reach the asymptotic part of the radial mean squared displacement in Eq. (11).

For a dual-porosity system (i.e., vermiculite; Fig. 1a), the water probes diffuse both in the interparticle ($\varepsilon_{interp.}$) and interlayer ($\varepsilon_{interl.}$) pore spaces. For the generated VPM, the porosity contribution arising from the interlayer space is thus estimated from the clay swelling properties through the c* crystallographic parameter (i.e., layer-to-layer distance) increasing from 10 Å in the dehydrated state to 14.86 Å in water-saturated conditions (Asaad et al., 2021; Faurel, 2012). $\varepsilon_{interl.}$ thus represents one-third of the solid clay phase ($\varepsilon_{interl.} = (1 - \varepsilon_{interp.})/3$), and the overall porosity ε is then given by (Table S1):

$$\varepsilon = \varepsilon_{interp.} + \varepsilon_{interl.} = \varepsilon_{interp.} + (1 - \varepsilon_{interp.})/3 \quad . \tag{12}$$

The same time step and simulation time as for water diffusion in single-porosity systems was considered. According to the porosity distribution in Eq. (12), the initialization of BD simulations was performed by randomly introducing the 2000 water probes in the VPM with an acceptance probability of 1/3 when the probe was included in the solid (i.e., to respect the water concentration between solid and interparticle porosity). The water tracer mobilities during BD simulations were treated as proposed by Asaad et al. (2021) for dual-porosity media. Briefly, water probes colliding with the basal and flat surface of the particles were allowed to rebound according to Maxwell's A wall, whereas a specific condition occurred in the case where the probe was in contact with a lateral surface of the particles. For this condition, the

probe was allowed to penetrate (or leave) the interlayer space of the particle according to the acceptance rule (Asaad et al., 2021; Bacle et al., 2016):

$$p_{acc}^{i\to j} = \min\left[1; \frac{p^j}{p^i} \times \frac{p_{gen}^{j\to i}}{p_{gen}^{i\to j}}\right] = \min\left[1; \frac{c_j}{c_i} \times \left(\frac{D_i}{D_j}\right)^{3/2} \times \exp\left(-\frac{\mathrm{d}^2}{4D_j\delta t} + \frac{\mathrm{d}^2}{4D_i\delta t}\right)\right] \quad , \tag{13}$$

where d is the modulus of the displacement from Eq. (10), and c_i and c_j are the water probe concentrations in environments i and j, respectively, with self-diffusion coefficients D_i and D_j. Such an acceptance rule allows preserving the respective concentrations of water tracers between interparticle and interlayer volumes during whole simulation timespan. The calculations require defining a water diffusion coefficient for the interlayer that was set to $D_{interl.} = 2.3.10^{-10}$ m^2 s^{-1}, which is approximately one order of magnitude lower than that of bulk water. This value is in agreement with numerical molecular dynamics results and experimental quasi-elastic neutron scattering results obtained for tetrahedrally charged trioctahedral saponite with similar layer charges (Asaad et al., 2021; Michot et al., 2012). At the end of the BD simulations, the pore water diffusion coefficients were extracted using Eq. (11).

3. Results

3.1. Structural and geometrical properties of virtual porous media

The consistency of the generated VPM can be further assessed through the analysis of their obtained orientation distribution functions. Indeed, different ODFs (and thus $f(\theta)$ functions) can lead, in principle, to the same $\langle P_2 \rangle$ parameter (Dabat et al., 2019). To do so, the ODFs were extracted and compared for different VPMs showing the same $\langle P_2 \rangle$ but different $\varepsilon_{interp.}$ values. As illustrated in Fig. 2a for $\langle P_2 \rangle \sim 0.57$, the ODFs extracted in the $0.25 \leq \varepsilon_{interp.} \leq 0.50$ interparticle porosity range were found to be identical, demonstrating the correct generation of different VPMs with the same geometrical and structural properties (particle size, distribution, and orientation) of the solid phase and a lack of bias during the construction procedure. Furthermore, these ODFs fully agree with the general orientation distribution function $f_{\mathrm{CM}}(\theta)$ determined by Dabat et al. (2019) on a wide range of natural clay-rich media (Fig. 2a), further demonstrating the representativeness of the VPM to represent real clay systems.

To investigate the relationship between the anisotropy of the solid phase (through the $\langle P_2 \rangle$ parameter) and that of the pore space, a chord length distribution analysis can be performed. This method is commonly used for a morphological description of the solid-pore interface (Dabat et al., 2018; Ferrage et al., 2015; Levitz and Tchoubar, 1992; Torquato and Lu, 1993). Accordingly, chords are line segments at the pore-solid interface for any direction r, lying

entirely in the pore (or solid) phase. For the pore space of a single-porosity system, the pore chord distribution function $f_p(r)$ is defined such that $f_p(r)dr$ represents the probability of having in the VPM a chord in the pore space of a length between r and $r + dr$ and by:

$$\int_0^\infty f_p(r)dr = 1 \quad . \tag{14}$$

A more easily handled quantity is the mean pore chord length ℓ along one scalar direction of the VPM (i.e., *x*, *y*, or *z*; Fig. 1d) and extracted from the first momentum of the $f_p(r)$ function as:

$$\ell = \int_0^\infty r\, f_p(r)dr \quad . \tag{15}$$

For all generated VPMs, the anisotropy of the pore space is thus quantified through the quantity $\ell_z/\ell_{\overline{xy}}$, i.e., the ratio between the mean pore chord length along the *z* direction and that along the *x* or *y* directions. Calculations were performed using 3D voxelized and binarized images (512^3 resolution), and $\ell_z/\ell_{\overline{xy}}$ values are reported in Table S1 for the 56 VPMs. As illustrated in Fig. 2b, the evolution of the $\ell_z/\ell_{\overline{xy}}$ ratio shows an almost linear relationship with the $\langle P_2 \rangle$ parameter. Moreover, the evolution is independent of the porosity value (Fig. 2b), and the slight increase in the $\ell_z/\ell_{\overline{xy}}$ ratio when decreasing porosity is assigned to the resolution that tends to make the segmentation of small slit-shaped pores in dense media difficult.

3.2. Comparison between experimental and calculated water diffusion data

The comparison between the experimental and calculated effective diffusion coefficients for water is shown in Fig. 3 through the *z* direction of the sample and as a mean value between the *x* and *y* directions (data reported in Table 1 and Table S1 for experimental and simulated data, respectively) for both single-porosity (i.e., kaolinite or illite) and dual-porosity media (i.e., vermiculite). In this representation, pore diffusion coefficients extracted from BD simulations are transformed into effective diffusion coefficients using Eq. (1) (Table S1). Overall, the simulated data appear to be in fair agreement with the experimental data, thus showing the efficiency of BD calculations on VPM to capture the observed trends and to account for the impact of porosity, anisotropy, and single- *vs*. dual-porosity on the water diffusion process. Note that for illite, or to a lesser extent for vermiculite, the simulated data appear to slightly overestimate D_{ez} values. This difference could be tentatively due to the lack of consideration of interfacial effects in the simulation, such as the reduction of water molecules for the charged external surfaces of clay minerals (Bourg and Tournassat, 2015). This effect remains, however, marginal compared to the role played by other parameters on the water diffusion process.

The evolution of the calculated D_e values with the $\langle P_2 \rangle$ parameter provides two noticeable findings. First, even though the D_{pz} values are strongly decreased for dual-porosity compared to single-porosity systems owing to the mobility reduction in the clay interlayers (Table S1), the transformation into D_{ez} values using Eq. (1) leads for a given $\varepsilon_{interp.}$ to similar effective

water mobilities for both single- and dual-porosity media (Fig. 3). Second, the D_e *vs.* $\langle P_2 \rangle$ evolution shows a linear trend, irrespective of the direction analyzed, which somehow recalls the steady increase in the anisotropy of the pore space with the preferred orientation of clay particles shown in Fig. 2b. The anisotropy of water diffusion, calculated through the ratio $D_{e\overline{xy}}/D_{ez}$ and plotted as a function of the $\langle P_2 \rangle$ parameter for single-porosity media in Fig. 4, is consistent with experimental diffusion data obtained for kaolinite (Table 1; (Asaad, 2021; Dabat et al., 2020). Data for dual-porosity media show the same evolution (Table S1). As previously noted for the $\ell_z/\ell_{\overline{xy}}$ *vs.* $\langle P_2 \rangle$ evolution (Fig. 2b), the anisotropy of water diffusion is independent of the porosity (Fig. 4).

4. Discussion

4.1. Close connection between the preferred orientation of particles and pore-space water diffusion

The BD calculations performed in the present study shed light on the role played by porosity, type of porosity, and degree of preferred orientation of clay particles on the diffusion of water in homogeneous clay-rich media. The fair agreement between the experimental and calculated diffusion data (Fig. 3) also fully validates the representativeness of the VPM for clay systems. Notably, these VPMs having micrometer-sized dimensions should in principle be limited to account for the actual heterogeneity in the distribution of porosity, particle orientation and size in a real centimeter-sized sample. However, this study shows that adjusting the bulk macroscopic properties of the solid phase (i.e., porosity, particle size, and $\langle P_2 \rangle$ parameter) into a small representative elementary volume is sufficient. In that regard, the generated VPM may not represent any part of the compacted sample that can be observed through imaging techniques (Gaboreau et al., 2016) but rather account for a representative virtual laboratory for analyzing specific processes occurring in the pore space.

The present study showed that several parameters, such as the anisotropy of the pore space or that of water diffusion coefficients, can be directly linked to the $\langle P_2 \rangle$ parameter, irrespective of the porosity value (Figs. 2b, 4). This provides a paradigm change, as transfer properties are commonly approached through the analysis of pore network organization, whereas parameter correlations are rather baseb here on the organization of the solid phase. Another key finding of the present work is that the consideration of additional interlayer porosity for a given $\varepsilon_{interp.}$ and $\langle P_2 \rangle$ value has a negligible influence on the overall D_e values even though D_p coefficients are strongly decreased for dual-porosity compared to single-porosity media (Fig. 3). This effect, previously reported by other authors (Asaad et al., 2021; Tyagi et al., 2013) for similar porosity ranges, demonstrates for dual-porosity media through Eq. (1) that the reduced overall pore

mobility is fully compensated by the increased diffusional volume. In other words, the strongly reduced mobility in the interlayer pores makes them act as dead volumes in the overall diffusional flux. It should be noted, however, that for lower porosity values compared to those investigated here, the reduction in interparticle porosity and thus the remaining presence of only small nanopores ensuring the connectivity of the pore network should lead to a noticeable difference in water diffusion between single-porosity and dual-porosity media (Tyagi et al., 2013; Van Loon and Mibus, 2015). In that regard, it should be kept in mind that the computational method considered in the present study does not consider the reduction of water molecules dynamics at the vicinity of the clay external surfaces. Although, the good agreement between experimental and simulated data likely pleads for a limited contribution of this effect for the porosity values investigated here, the situation may differ for very dense clay porous media.

4.2. Modification of the Archie model to account for the preferred orientation of clay particles

Owing to the lack of contribution of interlayer porosities on D_e/D_0 values for the range of porosity, the refinement of the Archie model described in Eq. (3) is based only on interparticle porosity, i.e., $\varepsilon_{interp.}$, rather than on the ε value. In Fig. 5a, the D_{ez}/D_0 evolution with $\varepsilon_{interp.}$ is shown for a few selected $\langle P_2 \rangle$ parameter series. Interestingly, for the most isotropic series (i.e., $\langle P_2 \rangle \sim 0.03$), the Archie model proposed by Tyagi et al. (2013) for isotropic systems is shown to be highly consistent with data obtained in the present study. These authors used computed bidimensional arrangements of clay grains, and the good agreement indicates that simulation for single-porosity media leads to similar results either based on 2D or 3D models.

To build a refined Archie model that accounts for the $\langle P_2 \rangle$ parameter, one may first consider the same relation $D_{ez}/D_0 = 0.48{\varepsilon_{interp.}}^{1.2}$ as Tyagi et al. (2013) to correctly predict the evolution of D_{ez}/D_0 (and $D_{e\overline{xy}}/D_0$) values for $\langle P_2 \rangle$=0. As a second step, one can exploit the steady linear decrease in D_{ez}/D_0 with $\langle P_2 \rangle$ shown in Fig. 3 to extract the slope of D_{ez}/D_0 as a function of the $\langle P_2 \rangle$ parameter for different $\varepsilon_{interp.}$ series (Fig. S1a). These slopes are found to be dependent on the $\varepsilon_{interp.}$ value (Fig. S1b), thus leading to the simple general formula:

$$D_{ez}/D_0 = 0.48{\varepsilon_{interp.}}^{1.2} - 0.272\langle P_2 \rangle \varepsilon_{interp.} \quad (16)$$

According to the relation of water diffusion anisotropy $D_{e\overline{xy}}/D_{ez}$ with the $\langle P_2 \rangle$ parameter (Fig. 4):

$$D_{e\overline{xy}}/D_{ez} = exp^{1.55\langle P_2 \rangle} \quad (17)$$

The prediction of the $D_{e\overline{xy}}/D_0$ value can be written as:

$$D_{e\overline{xy}}/D_0 = \left[0.48{\varepsilon_{interp.}}^{1.2} - 0.272\langle P_2 \rangle \varepsilon_{interp.}\right] exp^{1.55\langle P_2 \rangle} \quad (18)$$

In Fig. 5b, the original D_e/D_0 values derived from BD simulations are compared to those predicted using this proposed refined version of the Archie model. This comparison leads to a 1:1 relation with a correlation parameter of R^2=0.98, falling within the 15% uncertainty of D_e values (Fig. 3) and allowing a correct prediction of the entire dataset (Fig. 5c). Such a relation is established for single-porosity media but remains valid in the range of porosities investigated for dual-porosity media. For the latter case, one has to correctly assess the respective amounts of $\varepsilon_{interp.}$ and $\varepsilon_{interl.}$ quantities in the sample and to consider the $\varepsilon_{interp.}$ value in Eq. (16).

4.3. Toward a better safety prediction and design of barriers for waste management

The modified Archie model can be used to predict key aspects of the control of the preferred orientation of clay particles on water diffusional properties. As an example, for $\varepsilon_{interp.}$ = 0.40, the increase in preferred particle orientation from $\langle P_2 \rangle$=0 to $\langle P_2 \rangle$=1 reduced the D_{ez}/D_0 value by a factor of 3.5, which has the same impact as reducing $\varepsilon_{interp.}$ down to 0.15 (dashed arrows on Fig. 5c). Such a simple calculation sheds light on the need for consideration of preferred particle orientation in the prediction of water mobility in risk assessment and/or hazardous waste management containing clay materials.

The results obtained in the present study is of interest in the case of nuclear waste disposals, such as those envisaged in France in polymineralic argillaceous rocks (Callovo-Oxfordian formation). For this clay-rich formation, an overall experimental anisotropy of water diffusion $D_{e\overline{xy}}/D_{ez}$ between 1.5 and 2 has been reported (Robinet et al., 2012; Van Loon et al., 2004; Wenk et al., 2008). The results from mesoscopic water diffusion simulations performed by Robinet et al. (2012) considering an isotropic clay matrix (clay content ~50%) revealed the role played by elongated clay matrix distribution and non-clay grains on the anisotropy of water diffusion. These authors showed an anisotropic behavior of water diffusion in the simulations ($1.11<D_{e\overline{xy}}/D_{ez}<1.26$) resulting from the presence of elongated quartz or carbonate grains but lower than that obtained experimentally for tritiated water ($1.5<D_{e\overline{xy}}/D_{ez}<2.0$). As stated by these authors, the difference between experimental and simulated data could result from the lack of consideration of the preferred orientation of clay particles in the clay matrix. To go further, one may use the results of the present work to quantitatively assess the role played by clay orientation on the overall water diffusion process in these complex polymineralic samples. Dabat et al.,(2019) indeed recently measured the $\langle P_2 \rangle$ parameter of clays in the Callovo-Oxfordian formation at $\langle P_2 \rangle$=0.22, thus corresponding to $D_{e\overline{xy}}/D_{ez}$=1.41 according to Eq. (17). In a straightforward two-scale model, the overall anisotropy ratio can be assumed to be a product of the $D_{e\overline{xy}}/D_{ez}$ values resulting from the clay platelet orientation in the clay matrix ($D_{e\overline{xy}}/D_{ez}$=1.41) and textural elongation of the clay matrix ($1.11<D_{e\overline{xy}}/D_{ez}<1.26$), leading here to $1.56<D_{e\overline{xy}}/D_{ez}<1.73$, in agreement with the experimental water diffusion data. In this

regard, the refined model presented here paves the way for including both structural (orientation of particles) and textural (distribution of clay phases) properties for an accurate upscaling strategy for water diffusion, up to the centimeter scale. Such a simple two-scale approach could be applied to other clay-rich samples representative of nuclear waste storage in Europe, some of them showing higher macroscopic anisotropy values for water (and other tracers) diffusion ($D_{e\overline{xy}}/D_{ez}$ up to ~6; Gimmi et al., 2014; Van Loon et al., 2004; Van Loon and Soler, 2004).

A second potential implication of the present study concerns the design of safe clay-rich barriers used for municipal wastes and environmental protection. Compacted clay liners are the classical liner material used in municipal solid waste landfills for limiting or inhibiting the migration of generated leachates into the environment. In these systems, clays are mainly swelling clays (i.e., Na-bentonite) in the form of a thin centimeter-sized layer and very low hydraulic conductivity ($<10^{-9}$ m.s^{-1}), leading to transport controlled by diffusion processes (Czurda, 2006; Das and Bharat, 2021). Several studies have demonstrated the benefit of incorporating other types of clay minerals (e.g., kaolinite, illite, or vermiculite) in the clay liner (Baldev et al., 2020; Das and Bharat, 2021; Karunaratne et al., 2001; Sivapullaiah and Lakshmikanthay, 2005). These additions showed both an improvement in the mechanical properties (i.e., plasticity and shrinkage effects) of the liners and a reduction in their effective costs by introducing local clay materials in third world countries (Karunaratne et al., 2001). The results from the present study provides quantitative insights into the potential benefit of controlling the orientation of clay platelets in the liners, as an efficient route for improving their properties. Although the practical aspects of the material design remain a challenging task, one may assume that by increasing preferential orientation of clay platelets, similar safety properties could then be obtained for a thinner liner from the perspective of cost reduction and sober use of natural mineral resources.

5. Conclusions

This study represents a novel contribution to the quantitative understanding of the impact of the preferred orientation of clay particles on the diffusion of water in clay-based natural and artificial materials.

The good agreement between experimental water diffusion experiments at the centimeter scale and Brownian dynamics simulations demonstrates that a correct description of the full pore network geometry and connectivity can be obtained by injecting bulk properties of the solid phase (particle geometry, orientation, and porosity) in a virtual micrometer-sized sample. The organization of the solid phase through an easily measured $\langle P_2 \rangle$ parameter provides direct information on the evolution of the anisotropy in pore-space morphology and D_{ez} values with the preferred orientation of clay particles, irrespective of the porosity of the samples. In

addition, the large set of results clearly illustrates that, at least for a large range of interparticle porosities, the interlayer volume plays a marginal role in the effective diffusion coefficients measured. A logical perspective of this work would be to investigate the role played by these different parameters on anion and cations diffusion. Such extension would thus require accounting for diffuse double layers volumes in the virtual porous media. This may provide key insights regarding the coupled influence of the geometric and geochemical effects on solute diffusion.

Although, all data were obtained on pure clay samples, the present study provides also some interesting new insights regarding the connection between the anisotropic behavior of water diffusion properties for a pure clay matrix and those of a complex natural clay-rich system, such as those envisaged in the context of nuclear waste storage. The presented two-scale approach based on structural (orientation of particles) and textural (distribution of clay phases) properties to upscale anisotropic behavior of water diffusion up to the centimeter scale is promising. Future work would be needed, however, in order to validate this approach, e.g., (i) by extending this approach to different type of clay rocks and (ii) by investigating the role played by structural and mineralogical heterogeneities at higher length scale (i.e., from the centimeter to the field).

Declaration of Competing Interest

The authors declare that they have no known competing financial interests or personal relationships that could have appeared to influence the work reported in this paper.

Acknowledgements

The results presented here were partly obtained on the “environmental mineralogy” platform at IC2MP. Dimitri Prêt is thanked for constructive discussions about diffusion in clay rocks. The authors are grateful to the CNRS interdisciplinary “défi Needs” program (Projects TRANSREAC & DARIUS), the H2020 European Joint Program EURAD (WP “Future” - grant ID 847593), the French government program “Investissements d’Avenir” (EUR INTREE, reference ANR-18-EURE-0010), and the European Union (ERDF) and “Région Nouvelle Aquitaine” for providing financial support for this study. The constructive comments from two reviewers are also greatly acknowledged.

References

Archie, G.E., 1942. The electrical resistivity log as an aid in determining some reservoir characteristics. Transactions of the AIME 146, 54–62.

Asaad, A., 2021. Influence of particles organization and dual porosity on the diffusion of water and solutes in clay porous media. Université de Poitiers, Poitiers

(France).
Asaad, A., Hubert, F., Dazas, B., Razafitianamaharavo, A., Brunet, J., Glaus, M.A., Savoye, S., Ferrage, E., Tertre, E., 2022. A baseline study of mineralogical and morphological properties of different size fractions of illite du Puy. Applied Clay Science 224, 106517. https://doi.org/10.1016/j.clay.2022.106517
Asaad, A., Hubert, F., Ferrage, E., Dabat, T., Paineau, E., Porion, P., Savoye, S., Gregoire, B., Dazas, B., Delville, A., Tertre, E., 2021. Role of interlayer porosity and particle organization in the diffusion of water in swelling clays. Applied Clay Science 207, 106089. https://doi.org/10.1016/j.clay.2021.106089
Bacle, P., Dufrêche, J.-F., Rotenberg, B., Bourg, I.C., Marry, V., 2016. Modeling the transport of water and ionic tracers in a micrometric clay sample. Applied Clay Science 123, 18–28. https://doi.org/10.1016/j.clay.2015.12.014
Baldev, D., Kumar, A., Chauhan, P., Muthukumar, M., Shukla, S.K., 2020. Hydraulic and volume change characteristics of compacted clay liner blended with exfoliated vermiculite. International Journal of Environment and Waste Management 25, 430–440. https://doi.org/10.1504/IJEWM.2020.107563
Bourg, I.C., Sposito, G., 2011. Molecular dynamics simulations of the electrical double layer on smectite surfaces contacting concentrated mixed electrolyte (NaCl–CaCl2) solutions. Journal of Colloid and Interface Science 360, 701–715. https://doi.org/10.1016/j.jcis.2011.04.063
Bourg, I.C., Tournassat, C., 2015. Chapter 6 - Self-Diffusion of Water and Ions in Clay Barriers, in: Tournassat, C., Steefel, C.I., Bourg, I.C., Bergaya, F. (Eds.), Developments in Clay Science. Elsevier, pp. 189–226. https://doi.org/10.1016/B978-0-08-100027-4.00006-1
Callaghan, P.T., 1991. Principles of Nuclear Magnetic Resonance Microscopy, Oxford Science Publications. ed. Corby.
Chandrasekhar, S., 1943. Stochastic Problems in Physics and Astronomy. Rev. Mod. Phys. 15, 1–89. https://doi.org/10.1103/RevModPhys.15.1
Charlet, L., Alt-Epping, P., Wersin, P., Gilbert, B., 2017. Diffusive transport and reaction in clay rocks: A storage (nuclear waste, CO2, H2), energy (shale gas) and water quality issue. Advances in Water Resources 106, 39–59. https://doi.org/10.1016/j.advwatres.2017.03.019
Czurda, K., 2006. Chapter 11.3 Clay Liners and Waste Disposal, in: Bergaya, F., Theng, B.K.G., Lagaly, G. (Eds.), Developments in Clay Science. Elsevier, pp. 693–701. https://doi.org/10.1016/S1572-4352(05)01022-6
Dabat, T., 2019. Anisotropie d'orientation des particules des milieux poreux argileux et implication sur la diffusion de l'eau. Université de Poitiers, Poitiers (France).
Dabat, T., Hubert, F., Paineau, E., Launois, P., Laforest, C., Grégoire, B., Dazas, B., Tertre, E., Delville, A., Ferrage, E., 2019. A general orientation distribution function for clay-rich media. Nat Commun 10, 5456. https://doi.org/10.1038/s41467-019-13401-0
Dabat, T., Mazurier, A., Hubert, F., Tertre, E., Grégoire, B., Dazas, B., Ferrage, E., 2018. Mesoscale Anisotropy in Porous Media Made of Clay Minerals. A Numerical Study Constrained by Experimental Data. Materials 11. https://doi.org/10.3390/ma11101972
Dabat, T., Porion, P., Hubert, F., Paineau, E., Dazas, B., Grégoire, B., Tertre, E., Delville, A., Ferrage, E., 2020. Influence of preferred orientation of clay particles on the diffusion of water in kaolinite porous media at constant porosity. Applied Clay Science 184, 105354.

https://doi.org/10.1016/j.clay.2019.105354
Das, P., Bharat, T.V., 2021. Kaolin based protective barrier in municipal landfills against adverse chemo-mechanical loadings. Scientific Reports 11, 10354. https://doi.org/10.1038/s41598-021-89787-z
Descostes, M., Blin, V., Bazer-Bachi, F., Meier, P., Grenut, B., Radwan, J., Schlegel, M.L., Buschaert, S., Coelho, D., Tevissen, E., 2008. Diffusion of anionic species in Callovo-Oxfordian argillites and Oxfordian limestones (Meuse/Haute–Marne, France). Applied Geochemistry 23, 655–677. https://doi.org/10.1016/j.apgeochem.2007.11.003
Faurel, M., 2012. Conception et mise en place d'expériences de diffusion de l'eau et de solutés dans des milieux poreux modèles d'argiles gonflantes. Universtié de Poitiers, Poitiers (France).
Ferrage, E., Hubert, F., Baronnet, A., Grauby, O., Tertre, E., Delville, A., Bihannic, I., Prêt, D., Michot, L.J., Levitz, P., 2018. Influence of crystal structure defects on the small-angle neutron scattering/diffraction patterns of clay-rich porous media. Journal of Applied Crystallography 51, 1311–1322. https://doi.org/10.1107/S160057671801052X
Ferrage, E., Hubert, F., Tertre, E., Delville, A., Michot, L.J., Levitz, P., 2015. Modeling the arrangement of particles in natural swelling-clay porous media using three-dimensional packing of elliptic disks. Phys. Rev. E 91, 062210. https://doi.org/10.1103/PhysRevE.91.062210
Gaboreau, S., Robinet, J.-C., Prêt, D., 2016. Optimization of pore-network characterization of a compacted clay material by TEM and FIB/SEM imaging. Microporous and Mesoporous Materials 224, 116–128. https://doi.org/10.1016/j.micromeso.2015.11.035
Gimmi, T., Leupin, O.X., Eikenberg, J., Glaus, M.A., Van Loon, L.R., Waber, H.N., Wersin, P., Wang, H.A.O., Grolimund, D., Borca, C.N., Dewonck, S., Wittebroodt, C., 2014. Anisotropic diffusion at the field scale in a 4-year multi-tracer diffusion and retention experiment – I: Insights from the experimental data. Geochimica et Cosmochimica Acta 125, 373–393. https://doi.org/10.1016/j.gca.2013.10.014
Glaus, M.A., Frick, S., Rossé, R., Loon, L.R.V., 2010. Comparative study of tracer diffusion of HTO, 22Na+ and 36Cl− in compacted kaolinite, illite and montmorillonite. Geochimica et Cosmochimica Acta 74, 1999–2010. https://doi.org/10.1016/j.gca.2010.01.010
Holmboe, M., Bourg, I.C., 2014. Molecular Dynamics Simulations of Water and Sodium Diffusion in Smectite Interlayer Nanopores as a Function of Pore Size and Temperature. J. Phys. Chem. C 118, 1001–1013. https://doi.org/10.1021/jp408884g
Karunaratne, G.P., Chew, S.H., Lee, S.L., Sinha, A.N., 2001. Bentonite:Kaolinite Clay Liner. Geosynthetics International 8, 113–133. https://doi.org/10.1680/gein.8.0189
Kim, A.S., Chen, H., 2006. Diffusive tortuosity factor of solid and soft cake layers: A random walk simulation approach. Journal of Membrane Science 279, 129–139. https://doi.org/10.1016/j.memsci.2005.11.042
Levitz, P., Tchoubar, D., 1992. Disordered porous solids : from chord distributions to small angle scattering. J. Phys. I France 2, 771–790. https://doi.org/10.1051/jp1:1992174
Mazurek, M., Gautschi, A., Marschall, P., Vigneron, G., Lebon, P., Delay, J., 2008. Transferability of geoscientific information from various sources (study sites,

underground rock laboratories, natural analogues) to support safety cases for radioactive waste repositories in argillaceous formations. Physics and Chemistry of the Earth, Parts A/B/C 33, S95–S105. https://doi.org/10.1016/j.pce.2008.10.046

Michot, L.J., Ferrage, E., Jiménez-Ruiz, M., Boehm, M., Delville, A., 2012. Anisotropic Features of Water and Ion Dynamics in Synthetic Na- and Ca-Smectites with Tetrahedral Layer Charge. A Combined Quasi-elastic Neutron-Scattering and Molecular Dynamics Simulations Study. J. Phys. Chem. C 116, 16619–16633. https://doi.org/10.1021/jp304715m

Nakazawa, Y., Abe, T., Matsui, Y., Shinno, K., Kobayashi, S., Shirasaki, N., Matsushita, T., 2021. Differences in removal rates of virgin/decayed microplastics, viruses, activated carbon, and kaolin/montmorillonite clay particles by coagulation, flocculation, sedimentation, and rapid sand filtration during water treatment. Water Research 203, 117550. https://doi.org/10.1016/j.watres.2021.117550

Porion, P., Asaad, A., Dabat, T., Dazas, B., Delville, A., Ferrage, E., Hubert, F., Jiménez-Ruiz, M., Michot, L.J., Savoye, S., Tertre, E., 2021. Water and Ion Dynamics in Confined Media: A Multi-Scale Study of the Clay/Water Interface. Colloids and Interfaces 5. https://doi.org/10.3390/colloids5020034

Porion, P., Ferrage, E., Hubert, F., Tertre, E., Dabat, T., Faugère, A.M., Condé, F., Warmont, F., Delville, A., 2018. Water Mobility within Compacted Clay Samples: Multi-Scale Analysis Exploiting 1H NMR Pulsed Gradient Spin Echo and Magnetic Resonance Imaging of Water Density Profiles. ACS Omega 3, 7399–7406. https://doi.org/10.1021/acsomega.8b01083

Reinholdt, M.X., Hubert, F., Faurel, M., Tertre, E., Razafitianamaharavo, A., Francius, G., Prêt, D., Petit, S., Béré, E., Pelletier, M., Ferrage, E., 2013. Morphological properties of vermiculite particles in size-selected fractions obtained by sonication. Applied Clay Science 77–78, 18–32. https://doi.org/10.1016/j.clay.2013.03.013

Robinet, J.-C., Sardini, P., Coelho, D., Parneix, J.-C., Prêt, D., Sammartino, S., Boller, E., Altmann, S., 2012. Effects of mineral distribution at mesoscopic scale on solute diffusion in a clay-rich rock: Example of the Callovo-Oxfordian mudstone (Bure, France). Water Resources Research 48. https://doi.org/10.1029/2011WR011352

Rosanne, M., Mammar, N., Koudina, N., Prunet-Foch, B., Thovert, J.-F., Tevissen, E., Adler, P.M., 2003. Transport properties of compact clays: II. Diffusion. Journal of Colloid and Interface Science 260, 195–203. https://doi.org/10.1016/S0021-9797(02)00240-0

Sayed Hassan, M., Villieras, F., Gaboriaud, F., Razafitianamaharavo, A., 2006. AFM and low-pressure argon adsorption analysis of geometrical properties of phyllosilicates. Journal of Colloid and Interface Science 296, 614–623. https://doi.org/10.1016/j.jcis.2005.09.028

Sivapullaiah, P.V., Lakshmikanthay, H., 2005. Lime-stabilised illite as a liner. Proceedings of the Institution of Civil Engineers - Ground Improvement 9, 39–45. https://doi.org/10.1680/grim.2005.9.1.39

Tertre, E., Dazas, B., Asaad, A., Ferrage, E., Grégoire, B., Hubert, F., Delville, A., Delay, F., 2021. Connecting molecular simulations and laboratory experiments for the study of time-resolved cation-exchange process in the interlayer of swelling clay minerals. Applied Clay Science 200, 105913. https://doi.org/10.1016/j.clay.2020.105913

695 Tertre, E., Savoye, S., Hubert, F., Prêt, D., Dabat, T., Ferrage, E., 2018. Diffusion of
696 Water through the Dual-Porosity Swelling Clay Mineral Vermiculite. Environ.
697 Sci. Technol. 52, 1899–1907. https://doi.org/10.1021/acs.est.7b05343
698 Tinnacher, R.M., Holmboe, M., Tournassat, C., Bourg, I.C., Davis, J.A., 2016. Ion
699 adsorption and diffusion in smectite: Molecular, pore, and continuum scale
700 views. Geochimica et Cosmochimica Acta 177, 130–149.
701 https://doi.org/10.1016/j.gca.2015.12.010
702 Torquato, S., Lu, B., 1993. Chord-length distribution function for two-phase random
703 media. Phys. Rev. E 47, 2950–2953.
704 https://doi.org/10.1103/PhysRevE.47.2950
705 Tyagi, M., Gimmi, T., Churakov, S.V., 2013. Multi-scale micro-structure generation
706 strategy for up-scaling transport in clays. Advances in Water Resources 59,
707 181–195. https://doi.org/10.1016/j.advwatres.2013.06.002
708 Valleau, J.P., Diestler, D.J., Cushman, J.H., Schoen, M., Hertzner, A.W., Riley, M.E.,
709 1991. Comment on: Adsorption and diffusion at rough surfaces. A comparison
710 of statistical mechanics, molecular dynamics, and kinetic theory. J. Chem.
711 Phys. 95, 6194–6195. https://doi.org/10.1063/1.461595
712 van Gunsteren, W.F., Berendsen, H.J.C., Rullmann, J.A.C., 1981. Stochastic dynamics
713 for molecules with constraints. Molecular Physics 44, 69–95.
714 https://doi.org/10.1080/00268978100102291
715 Van Loon, L.R., Baeyens, B., Bradbury, M.H., 2005. Diffusion and retention of
716 sodium and strontium in Opalinus clay: Comparison of sorption data from
717 diffusion and batch sorption measurements, and geochemical calculations.
718 Applied Geochemistry 20, 2351–2363.
719 https://doi.org/10.1016/j.apgeochem.2005.08.008
720 Van Loon, L.R., Mibus, J., 2015. A modified version of Archie's law to estimate
721 effective diffusion coefficients of radionuclides in argillaceous rocks and its
722 application in safety analysis studies. Applied Geochemistry 59, 85–94.
723 https://doi.org/10.1016/j.apgeochem.2015.04.002
724 Van Loon, L.R., Soler, J.M., 2004. Diffusion of HTO, 36Cl−, 125I− and 22Na+ in
725 Opalinus Clay: Effect of confining pressure, sample orientation, sample depth
726 and temperature. Paul Scherrer Insitut, Villigen, Switzerland.
727 Van Loon, L.R., Soler, J.M., Müller, W., Bradbury, M.H., 2004. Anisotropic Diffusion
728 in Layered Argillaceous Rocks: A Case Study with Opalinus Clay. Environ.
729 Sci. Technol. 38, 5721–5728. https://doi.org/10.1021/es049937g
730 Wang, M., Orr, A.A., Jakubowski, J.M., Bird, K.E., Casey, C.M., Hearon, S.E.,
731 Tamamis, P., Phillips, T.D., 2021. Enhanced adsorption of per- and
732 polyfluoroalkyl substances (PFAS) by edible, nutrient-amended
733 montmorillonite clays. Water Research 188, 116534.
734 https://doi.org/10.1016/j.watres.2020.116534
735 Wenk, H.-R., Voltolini, M., Mazurek, M., Van Loon, L.R., Vinsot, A., 2008. Preferred
736 orientations and anisotropy in shales: Callovo-Oxfordian shale (France) and
737 Opalinus Clay (Switzerland). Clays and Clay Minerals 56, 285–306.
738 https://doi.org/10.1346/CCMN.2008.0560301
739 Wu, T., Dai, W., Xiao, G.P., Shu, F.J., Yao, J., Li, J.Y., 2012. Influence of dry density
740 on HTO diffusion in GMZ bentonite. Journal of Radioanalytical and Nuclear
741 Chemistry 292, 853–857. https://doi.org/10.1007/s10967-011-1523-y
742 Wu, T., Wang, H., Zheng, Q., Zhao, Y.L., Van Loon, L.R., 2014. Diffusion behavior of
743 Se(IV) and Re(VII) in GMZ bentonite. Applied Clay Science 101, 136–140.
744 https://doi.org/10.1016/j.clay.2014.07.028

Wu, T., Wang, Z., Tong, Y., Wang, Y., Van Loon, L.R., 2018. Investigation of Re(VII) diffusion in bentonite by through-diffusion and modeling techniques. Applied Clay Science 166, 223–229. https://doi.org/10.1016/j.clay.2018.08.023

Yan, B., Wang, J., Liu, J., 2021. STXM-XANES and computational investigations of adsorption of per- and polyfluoroalkyl substances on modified clay. Water Research 201, 117371. https://doi.org/10.1016/j.watres.2021.117371

Yang, X., An, C., Feng, Q., Boufadel, M., Ji, W., 2022. Aggregation of microplastics and clay particles in the nearshore environment: Characteristics, influencing factors, and implications. Water Research 224, 119077. https://doi.org/10.1016/j.watres.2022.119077

Ye, X., Cheng, Z., Wu, M., Hao, Y., Lu, G., Hu, B.X., Mo, C., Li, Q., Wu, Jianfeng, Wu, Jichun, 2022. Effects of clay minerals on the transport of polystyrene nanoplastic in groundwater. Water Research 223, 118978. https://doi.org/10.1016/j.watres.2022.118978

Figure Captions

Fig. 1. Description of clay porous media. (**a**) Crystal structure of kaolinite, illite and vermiculite. (**b-c**) Representation of single-porosity (e.g., kaolinite or illite) or dual-porosity (e.g., vermiculite) porous medium for water diffusion. (**d**) Spherical coordinates (θ, φ) defining the orientation of an individual clay platelet with respect to the laboratory frame. (**e**) Selected virtual porous media with a given value of interparticle porosity ($\varepsilon_{interp.}$) but different degrees of preferred orientation in clay particles ($\langle P_2 \rangle$ parameter). (**f**) Selected virtual porous media with an almost isotropic organization ($\langle P_2 \rangle = 0.03$) but different $\varepsilon_{interp.}$ values.

Fig. 2. Structural and geometrical properties of virtual porous media. (**a**) Comparison between different orientation distribution functions $f(\theta)$ extracted from virtual porous media with the same degree in preferred orientation of particles ($\langle P_2 \rangle \sim 0.57$) but different interparticle porosity $\varepsilon_{interp.}$ values. The extracted $f(\theta)$ functions are also compared with the generalized ODF for natural clay-rich media $f_{\mathrm{CM}}(\theta)$ (solid red line) as determined by Dabat et al. (2019). (**b**) Evolution of the anisotropy in the pore space through the mean chord length analysis and $\ell_z/\ell_{\overline{xy}}$ ratio with the degree in preferred orientation of clay particles ($\langle P_2 \rangle$ parameter).

Fig. 3. Brownian dynamics simulation of water diffusion in virtual porous media. The results are shown for single-porosity (left) or dual-porosity (right) types of diffusion as a function of the degree of preferred orientation in clay particles ($\langle P_2 \rangle$ parameter). D_e/D_0 values extracted along the z direction (D_{ez}/D_0) are shown as squares, whereas the mean values of effective diffusion coefficients along the x or y directions ($D_{e\overline{xy}}/D_0$) are shown as circles. Available experimental data from Table 1 are reported for kaolinite, illite, and vermiculite in orange, red, and green, respectively.

Fig. 4. Anisotropy in water diffusion for single-porosity media. Evolution of the anisotropy in the effective water diffusion coefficients ($D_{e\overline{xy}}/D_{ez}$ ratio) with the degree of preferred orientation of clay particles ($\langle P_2 \rangle$ parameter) for different interparticle porosity ($\varepsilon_{interp.}$) values. The solid red line indicates the best-fit relation (correlation Factor R^2=0.98). The orange diamonds correspond to experimental data obtained on kaolinite samples (Table 1; (Asaad et al., 2021; Dabat et al., 2020)).

Fig. 5. Modification of the Archie model to account for the preferred orientation of clay particles in the water diffusion process. (**a**) Evolution for single-porosity systems of water diffusion coefficients along the z direction (D_{ez}/D_0) as a function of interparticle porosity

($\varepsilon_{interp.}$) for the selected $\langle P_2 \rangle$ series. The dashed red line corresponds to the Archie model proposed by Tyagi et al. (2013) for isotropic clay media. (**b**) Comparison between D_e/D_0 values predicted using the modified Archie model proposed in this study and those derived from Brownian dynamics. D_e/D_0 values extracted along the *z* direction (D_{ez}/D_0) are shown as solid squares, whereas the mean values of effective diffusion coefficients along the *x* or *y* directions ($D_{e\overline{xy}}/D_0$) are shown as open circles. The solid line corresponds to a 1:1 relation, whereas dotted lines correspond to the 15% uncertainty envelope on D_e/D_0 values extracted from simulations. (**c**) Same as (a) with a projection of predicted (D_{ez}/D_0) using the modified Archie model proposed in this study for the selected $\langle P_2 \rangle$ series.

808

809 **Tables**

810

811 **Table 1**. Experimental water diffusion coefficient obtained on pure kaolinite, illite, or
812 vermiculite clay samples using through-diffusion experiments or pulse-gradient spin–echo
813 nuclear magnetic resonance spectroscopy

Clay type	$\varepsilon_{interp.}$ (±0.02)	$\varepsilon_{interl.}$ (±0.02)	ε (±0.02)	$\langle P_2 \rangle$ (±0.02)	Technique	D_{pz}/D_0	$D_{p\overline{xy}}/D_0$	D_{ez}/D_0	$D_{e\overline{xy}}/D_0$
Kaolinite	0.26	-	0.26	0.35[a]	TD	-	-	0.081[b]	-
	0.26	-	0.26	0.35[a]	PGSE-NMR	0.289[a]	0.356[a]	0.075	0.093
	0.36	-	0.36	0.25[c]	TD	-	-	0.129[c]	-
	0.38	-	0.38	0.24[c]	TD	-	-	0.110[c]	-
	0.50	-	0.50	0.21[d]	PGSE-NMR	0.426[d]	0.506[d]	0.213	0.253
	0.50	-	0.50	0.59[d]	PGSE-NMR	0.307[d]	0.586[d]	0.153	0.293
Illite	0.28	-	0.28	0.11[e]	TD	-	-	0.054[e]	-
	0.28	-	0.28	0.11[e]	TD	-	-	0.044[e]	-
	0.28	-	0.28	0.11[e]	TD	-	-	0.041[e]	-
	0.34	-	0.34	0.11[e]	TD	-	-	0.074[e]	-
	0.34	-	0.34	0.11[e]	TD	-	-	0.073[e]	-
	0.38	-	0.38	0.54[e]	TD	-	-	0.046[e]	-
Vermiculite	0.24	0.25	0.49	0.07[c]	TD	-	-	0.086[c]	-
	0.24	0.25	0.49	0.07[c]	TD	-	-	0.095[c]	-
	0.25	0.25	0.50	0.03[e]	TD	-	-	0.086[e]	-
	0.24	0.25	0.49	0.41[e]	TD	-	-	0.042[e]	-

Data from [a] (Asaad et al., 2021), [b] (Tertre et al., 2018), [c] (Dabat, 2019), [d] (Dabat et al., 2020), [e] (Asaad, 2021). All samples were prepared by compaction, excepted samples with $\langle P_2 \rangle$>0.4 that were prepared by centrifugation. TD and PGSE-NMR stand for through-diffusion experiments and pulse-gradient spin–echo nuclear magnetic resonance spectroscopy, respectively. Different D_{ez} values for the same porosity in [c] or [e] were obtained considering different ionic strengths for NaCl in TD experiments.

814

815

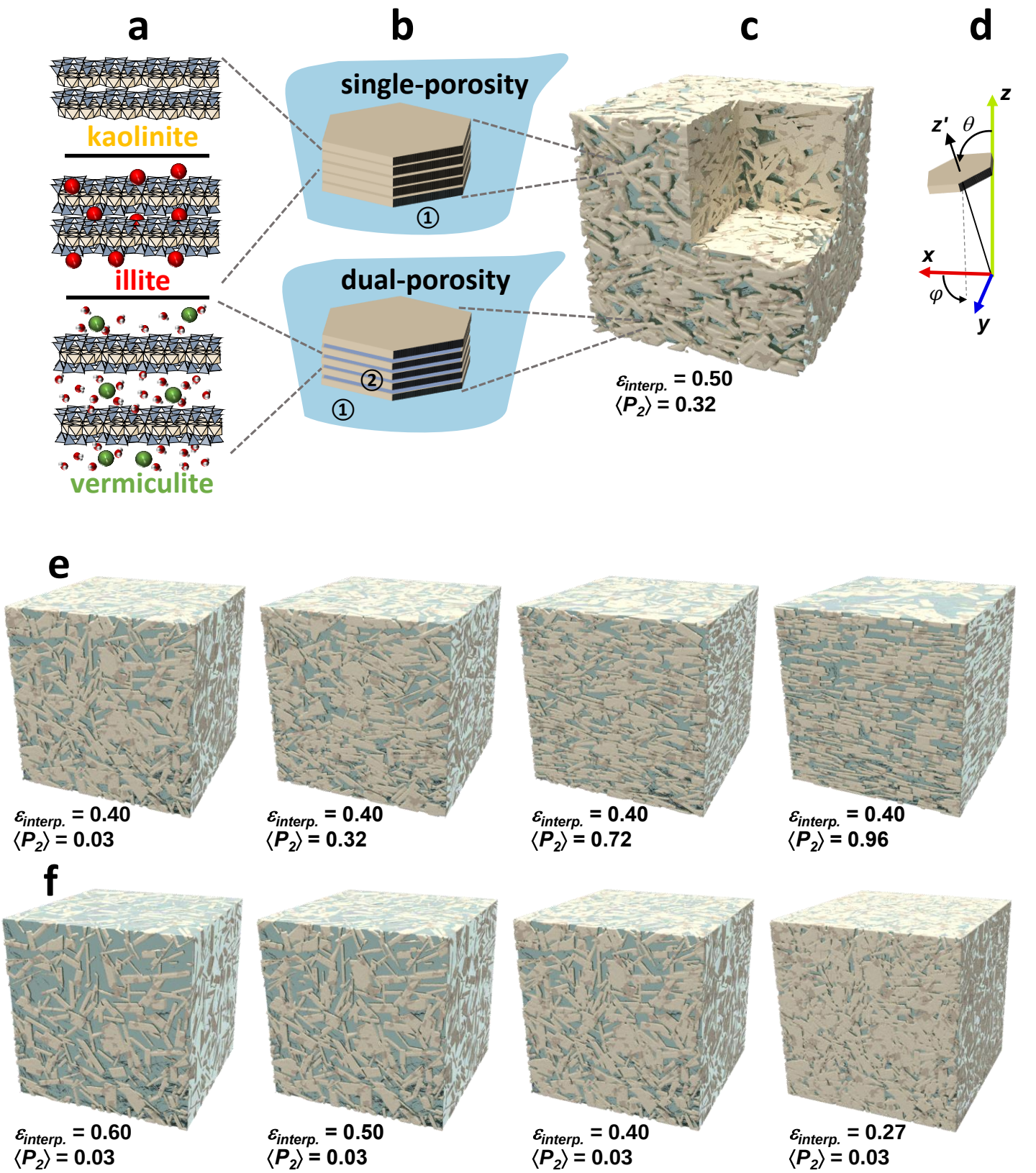
a
b
c
d
kaolinite
illite
vermiculite
single-porosity
dual-porosity
①
②
①
$\varepsilon_{interp.}$ = 0.50
$\langle P_2 \rangle$ = 0.32
z
z'
θ
x
φ
y
e
$\varepsilon_{interp.}$ = 0.40
$\langle P_2 \rangle$ = 0.03
$\varepsilon_{interp.}$ = 0.40
$\langle P_2 \rangle$ = 0.32
$\varepsilon_{interp.}$ = 0.40
$\langle P_2 \rangle$ = 0.72
$\varepsilon_{interp.}$ = 0.40
$\langle P_2 \rangle$ = 0.96
f
$\varepsilon_{interp.}$ = 0.60
$\langle P_2 \rangle$ = 0.03
$\varepsilon_{interp.}$ = 0.50
$\langle P_2 \rangle$ = 0.03
$\varepsilon_{interp.}$ = 0.40
$\langle P_2 \rangle$ = 0.03
$\varepsilon_{interp.}$ = 0.27
$\langle P_2 \rangle$ = 0.03

Fig. 01

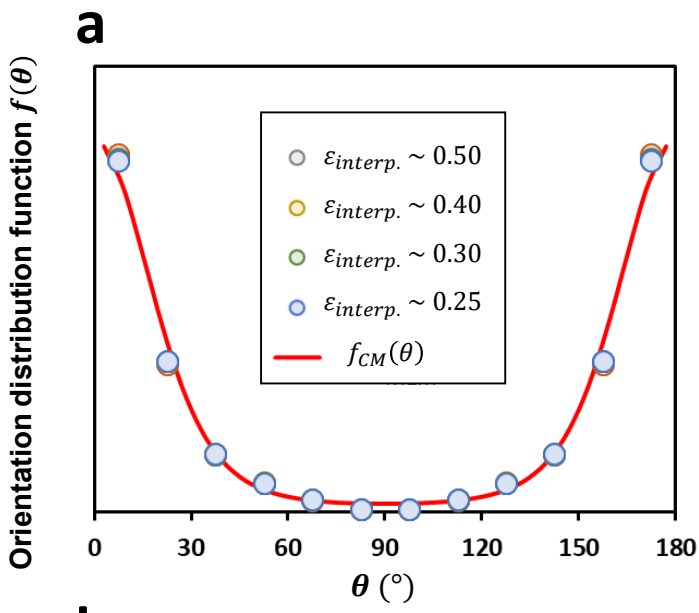
a
Orientation distribution function $f(\theta)$
$\varepsilon_{interp.} \sim 0.50$
$\varepsilon_{interp.} \sim 0.40$
$\varepsilon_{interp.} \sim 0.30$
$\varepsilon_{interp.} \sim 0.25$
$f_{CM}(\theta)$
0
30
60
90
120
150
180
θ (°)

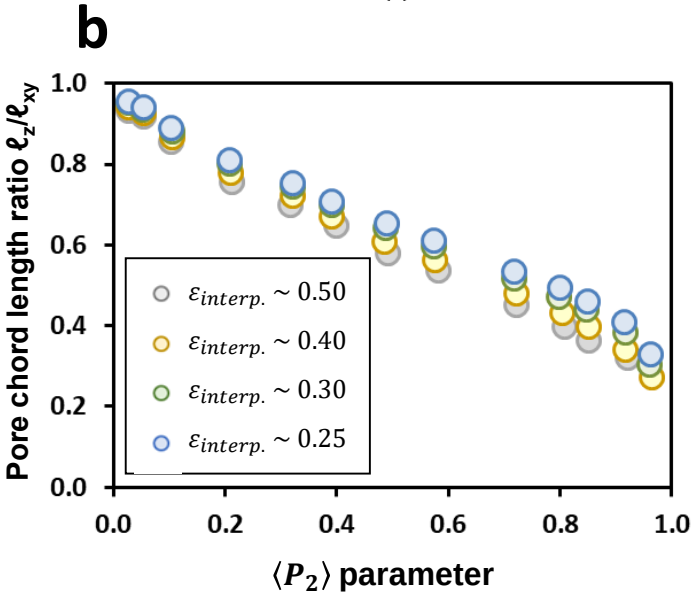
b
Pore chord length ratio ℓ_z/ℓ_{xy}
1.0
0.8
0.6
0.4
0.2
0.0
$\varepsilon_{interp.} \sim 0.50$
$\varepsilon_{interp.} \sim 0.40$
$\varepsilon_{interp.} \sim 0.30$
$\varepsilon_{interp.} \sim 0.25$
0.0
0.2
0.4
0.6
0.8
1.0
$\langle P_2 \rangle$ parameter

Fig. 02

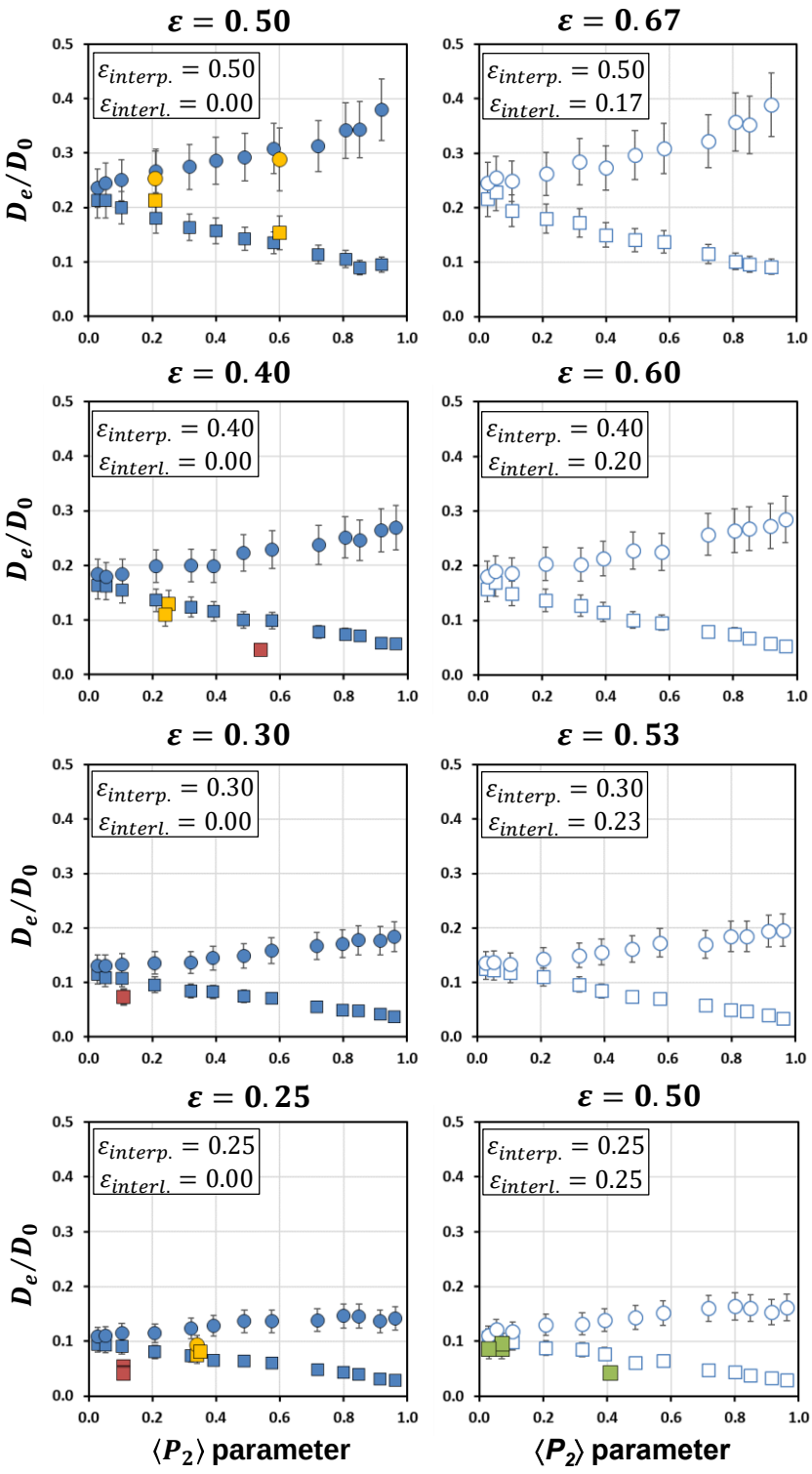
$\varepsilon = 0.50$
$\varepsilon_{interp.} = 0.50$
$\varepsilon_{interl.} = 0.00$
$\varepsilon = 0.67$
$\varepsilon_{interp.} = 0.50$
$\varepsilon_{interl.} = 0.17$
$\varepsilon = 0.40$
$\varepsilon_{interp.} = 0.40$
$\varepsilon_{interl.} = 0.00$
$\varepsilon = 0.60$
$\varepsilon_{interp.} = 0.40$
$\varepsilon_{interl.} = 0.20$
$\varepsilon = 0.30$
$\varepsilon_{interp.} = 0.30$
$\varepsilon_{interl.} = 0.00$
$\varepsilon = 0.53$
$\varepsilon_{interp.} = 0.30$
$\varepsilon_{interl.} = 0.23$
$\varepsilon = 0.25$
$\varepsilon_{interp.} = 0.25$
$\varepsilon_{interl.} = 0.00$
$\varepsilon = 0.50$
$\varepsilon_{interp.} = 0.25$
$\varepsilon_{interl.} = 0.25$
D_e/D_0
$\langle P_2 \rangle$ parameter
$\langle P_2 \rangle$ parameter

Fig. 03

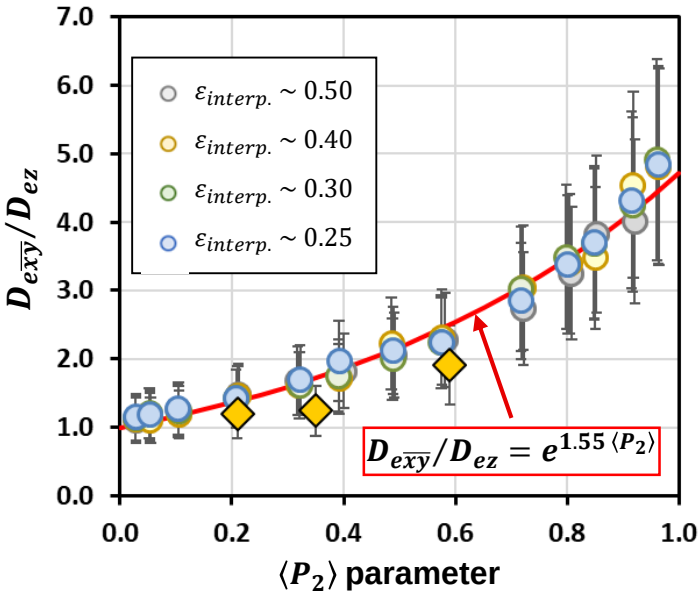
7.0
6.0
5.0
4.0
3.0
2.0
1.0
0.0
$D_{e\overline{xy}}/D_{ez}$
$\varepsilon_{interp.} \sim 0.50$
$\varepsilon_{interp.} \sim 0.40$
$\varepsilon_{interp.} \sim 0.30$
$\varepsilon_{interp.} \sim 0.25$
$D_{e\overline{xy}}/D_{ez} = e^{1.55\,\langle P_2 \rangle}$
0.0
0.2
0.4
0.6
0.8
1.0
$\langle P_2 \rangle$ parameter

Fig. 04

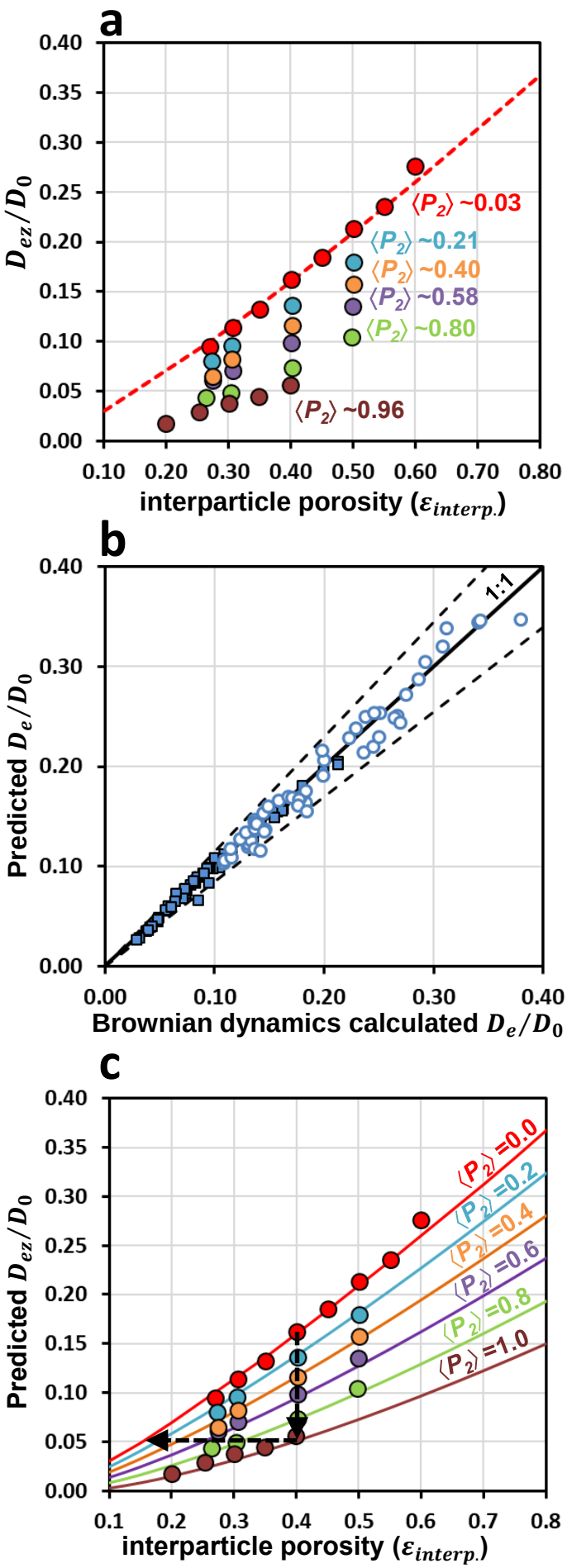
a
0.40
0.35
0.30
0.25
0.20
0.15
0.10
0.05
0.00
D_{ez}/D_0
⟨P2⟩ ~0.03
⟨P2⟩ ~0.21
⟨P2⟩ ~0.40
⟨P2⟩ ~0.58
⟨P2⟩ ~0.80
⟨P2⟩ ~0.96
0.10 0.20 0.30 0.40 0.50 0.60 0.70 0.80
interparticle porosity ($\varepsilon_{interp.}$)
b
0.40
0.30
0.20
0.10
0.00
Predicted D_e/D_0
1:1
0.00 0.10 0.20 0.30 0.40
Brownian dynamics calculated D_e/D_0
c
0.40
0.35
0.30
0.25
0.20
0.15
0.10
0.05
0.00
Predicted D_{ez}/D_0
⟨P2⟩=0.0
⟨P2⟩=0.2
⟨P2⟩=0.4
⟨P2⟩=0.6
⟨P2⟩=0.8
⟨P2⟩=1.0
0.1 0.2 0.3 0.4 0.5 0.6 0.7 0.8
interparticle porosity ($\varepsilon_{interp.}$)

Fig. 05

SUPPLEMENTARY INFORMATION

Anisotropy in particle orientation controls water diffusion in clay materials

Eric Ferrage[a]*, Fabien Hubert[a], Thomas Dabat[a], Ali Asaad[a], Baptiste Dazas[a], Brian Grégoire[a], Sébastien Savoye[b], Emmanuel Tertre[a]

[a] *IC2MP, Equipe HydrASA, UMR 7285 CNRS/Université de Poitiers, 86073 Poitiers, France,*

[b] *Université Paris-Saclay, CEA, DRMP-Service de Physico-Chimie, 91191 Gif-sur Yvette, France*

Contents

Table S1. Structural properties of the different virtual porous media generated and associated water diffusion coefficients obtained by Brownian dynamics on either single- or dual-porosity configurations

VPM series	$\varepsilon_{interp.}$	N	$\langle P_2 \rangle$	$\ell_z/\ell_{\overline{xy}}$	Single-porosity water diffusion					Dual-porosity water diffusion				
					ε	$\frac{D_{pz}}{D_0}$	$\frac{D_{p\overline{xy}}}{D_0}$	$\frac{D_{ez}}{D_0}$	$\frac{D_{e\overline{xy}}}{D_0}$	ε	$\frac{D_{pz}}{D_0}$	$\frac{D_{p\overline{xy}}}{D_0}$	$\frac{D_{ez}}{D_0}$	$\frac{D_{e\overline{xy}}}{D_0}$
$\langle P_2 \rangle \sim 0.03$														
	0.60	1748	0.03	0.92	0.60	0.461	0.531	0.276	0.318	0.73	0.380	0.441	0.279	0.323
	0.55	2167	0.03	0.93	0.55	0.428	0.488	0.236	0.269	0.70	0.358	0.388	0.251	0.272
	0.50	2692	0.03	0.93	0.50	0.426	0.471	0.213	0.236	0.67	0.324	0.369	0.216	0.246
	0.45	3383	0.03	0.94	0.45	0.411	0.461	0.185	0.208	0.63	0.305	0.322	0.193	0.204
	0.40	4325	0.03	0.94	0.40	0.406	0.458	0.163	0.184	0.60	0.262	0.301	0.157	0.181
	0.35	5762	0.03	0.95	0.35	0.377	0.446	0.132	0.156	0.57	0.247	0.275	0.140	0.156
	0.31	8056	0.03	0.95	0.31	0.372	0.425	0.114	0.131	0.54	0.232	0.252	0.125	0.136
	0.27	10639	0.03	0.95	0.27	0.348	0.399	0.095	0.109	0.51	0.207	0.215	0.107	0.111
$\langle P_2 \rangle \sim 0.05$														
	0.50	2841	0.05	0.92	0.50	0.425	0.490	0.212	0.245	0.67	0.342	0.383	0.228	0.255
	0.40	4552	0.05	0.93	0.40	0.401	0.443	0.162	0.179	0.60	0.281	0.315	0.169	0.190
	0.31	8402	0.05	0.94	0.31	0.353	0.425	0.109	0.131	0.54	0.227	0.256	0.122	0.138
	0.27	10932	0.05	0.94	0.27	0.339	0.400	0.093	0.110	0.51	0.196	0.235	0.101	0.121
$\langle P_2 \rangle \sim 0.10$														
	0.50	2743	0.10	0.85	0.50	0.398	0.501	0.199	0.250	0.67	0.291	0.373	0.194	0.249
	0.40	4470	0.10	0.87	0.40	0.385	0.457	0.155	0.184	0.60	0.248	0.310	0.149	0.187
	0.31	8357	0.10	0.88	0.31	0.352	0.435	0.108	0.133	0.54	0.218	0.249	0.117	0.134
	0.27	11039	0.10	0.89	0.27	0.335	0.425	0.091	0.115	0.51	0.192	0.228	0.099	0.117
$\langle P_2 \rangle \sim 0.20$														
	0.50	2825	0.21	0.75	0.50	0.360	0.534	0.180	0.267	0.67	0.269	0.393	0.180	0.262
	0.40	4636	0.21	0.78	0.40	0.338	0.494	0.136	0.199	0.60	0.227	0.338	0.136	0.204
	0.31	8056	0.21	0.80	0.31	0.313	0.444	0.096	0.136	0.54	0.205	0.266	0.110	0.143
	0.27	11139	0.21	0.81	0.27	0.296	0.421	0.081	0.115	0.51	0.171	0.253	0.088	0.130
$\langle P_2 \rangle \sim 0.32$														
	0.50	2771	0.32	0.70	0.50	0.327	0.549	0.163	0.275	0.67	0.258	0.425	0.172	0.284
	0.40	4592	0.32	0.72	0.40	0.308	0.498	0.124	0.200	0.60	0.211	0.337	0.127	0.203
	0.31	8680	0.32	0.75	0.31	0.276	0.447	0.084	0.137	0.54	0.180	0.279	0.096	0.150
	0.27	11307	0.32	0.75	0.27	0.268	0.454	0.073	0.124	0.51	0.164	0.256	0.085	0.132
$\langle P_2 \rangle \sim 0.39$														
	0.50	2785	0.40	0.65	0.50	0.314	0.572	0.157	0.286	0.67	0.224	0.410	0.150	0.273

0.40	4619	0.39	0.67	0.40	0.288	0.493	0.116	0.198	0.60	0.192	0.354	0.115	0.213
0.31	8728	0.39	0.70	0.31	0.270	0.473	0.083	0.145	0.54	0.157	0.290	0.085	0.156
0.28	11092	0.39	0.71	0.28	0.236	0.466	0.065	0.128	0.52	0.149	0.269	0.077	0.139

$\langle P_2 \rangle \sim 0.49$

0.50	2683	0.49	0.58	0.50	0.285	0.585	0.142	0.292	0.67	0.211	0.445	0.141	0.297
0.40	4428	0.49	0.61	0.40	0.249	0.555	0.100	0.223	0.60	0.167	0.378	0.101	0.227
0.31	8473	0.49	0.64	0.31	0.244	0.488	0.075	0.149	0.54	0.137	0.302	0.074	0.162
0.27	11139	0.49	0.65	0.27	0.236	0.500	0.064	0.136	0.52	0.130	0.278	0.061	0.143

$\langle P_2 \rangle \sim 0.57$

0.50	2736	0.58	0.54	0.50	0.270	0.616	0.135	0.308	0.67	0.207	0.462	0.138	0.308
0.40	4578	0.58	0.56	0.40	0.246	0.570	0.099	0.229	0.60	0.159	0.375	0.096	0.225
0.31	8834	0.57	0.60	0.31	0.232	0.518	0.071	0.159	0.54	0.130	0.322	0.070	0.173
0.28	11404	0.57	0.61	0.28	0.221	0.496	0.061	0.137	0.52	0.126	0.293	0.065	0.152

$\langle P_2 \rangle \sim 0.72$

0.50	2524	0.72	0.45	0.50	0.228	0.624	0.114	0.312	0.67	0.173	0.484	0.115	0.322
0.40	4269	0.72	0.48	0.40	0.195	0.593	0.078	0.238	0.60	0.132	0.428	0.079	0.257
0.31	8268	0.72	0.52	0.31	0.181	0.549	0.055	0.167	0.54	0.108	0.317	0.058	0.170
0.27	11446	0.72	0.54	0.27	0.180	0.514	0.048	0.138	0.51	0.093	0.312	0.048	0.160

$\langle P_2 \rangle \sim 0.80$

0.50	2466	0.81	0.40	0.50	0.210	0.682	0.105	0.341	0.67	0.152	0.537	0.101	0.357
0.40	4133	0.80	0.43	0.40	0.184	0.624	0.074	0.251	0.60	0.125	0.439	0.075	0.264
0.30	8095	0.80	0.47	0.30	0.162	0.564	0.049	0.171	0.54	0.093	0.345	0.050	0.185
0.26	11693	0.80	0.49	0.26	0.164	0.553	0.043	0.146	0.51	0.085	0.321	0.043	0.164

$\langle P_2 \rangle \sim 0.85$

0.50	2531	0.85	0.36	0.50	0.179	0.686	0.090	0.343	0.67	0.145	0.529	0.096	0.352
0.40	4226	0.85	0.40	0.40	0.176	0.611	0.071	0.246	0.60	0.112	0.446	0.068	0.268
0.30	8308	0.85	0.44	0.30	0.159	0.585	0.048	0.177	0.54	0.089	0.344	0.047	0.184
0.26	11863	0.85	0.46	0.26	0.149	0.551	0.039	0.146	0.51	0.074	0.315	0.038	0.161

$\langle P_2 \rangle \sim 0.92$

0.50	2490	0.92	0.32	0.50	0.189	0.759	0.095	0.380	0.67	0.138	0.585	0.092	0.389
0.40	3659	0.92	0.34	0.40	0.145	0.660	0.058	0.264	0.60	0.097	0.455	0.058	0.273
0.30	7116	0.92	0.38	0.30	0.137	0.584	0.042	0.177	0.53	0.074	0.364	0.040	0.194
0.25	11526	0.91	0.41	0.25	0.127	0.548	0.032	0.136	0.50	0.066	0.308	0.033	0.154

$\langle P_2 \rangle \sim 0.96$

0.40	2711	0.96	0.27	0.40	0.140	0.674	0.056	0.269	0.60	0.088	0.475	0.053	0.285
0.35	3562	0.96	0.29	0.35	0.129	0.636	0.045	0.222	0.57	0.080	0.427	0.045	0.241
0.30	4954	0.96	0.30	0.30	0.124	0.612	0.037	0.184	0.53	0.064	0.367	0.034	0.196

0.25	7403	0.96	0.33	0.25	0.116	0.559	0.029	0.142	0.50	0.058	0.321	0.029	0.161
0.20	10137	0.96	0.34	0.19	0.090	0.458	0.017	0.089	0.46	0.027	0.159	0.012	0.074

$\langle P_2 \rangle$ stands for the degree of preferred orientation, $\varepsilon_{interp.}$ is the interparticle porosity, N is the number of clay particles, and $\ell_z/\ell_{\overline{xy}}$ is the anisotropic ratio of mean pore lengths in the z or (x,y) directions. Water diffusion is characterized by an overall porosity ε ($\varepsilon = \varepsilon_{interp.}$ or $\varepsilon = \varepsilon_{interp.} + \varepsilon_{interl.}$ for single- or dual-porosity configurations, respectively), and pore diffusion coefficients D_p or effective diffusion coefficients D_e are normalized by the bulk self-diffusion of water D_0.

38

39

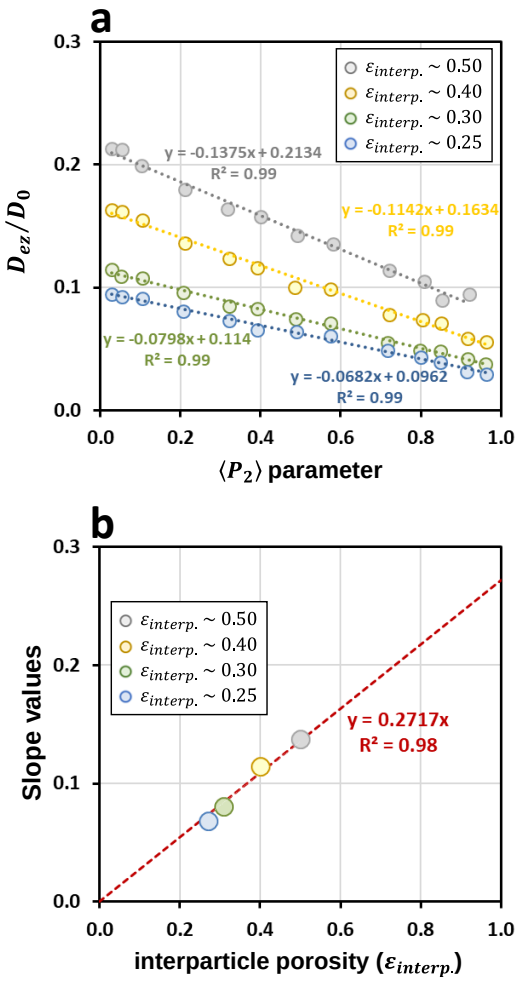

Fig. S1. Determination of the modified Archie model to account for the preferred orientation of clay particles in the water diffusion process. (**a**) Evolution of D_{ez}/D_0 values for single-porosity systems of water diffusion coefficients along the z direction (D_{ez}/D_0) with the degree of preferred orientation of clay particles ($\langle P_2 \rangle$ parameter; same as Fig. 3) for different interparticle porosity ($\varepsilon_{interp.}$) values and associated linear correlation parameters. (**b**) Evolution of the slopes obtained in (a) as a function of interparticle porosity and associated linear correlation parameters.